Title:

Giardia's ventral disc is hyperstable and composed of over 80 disc-associated proteins

Authors:

Nosala, C., Hagen, K.D., Jones, K. Loudermilk, R., Nguyen, K., and S.C. Dawson

Address:

Department of Microbiology and Molecular Genetics

One Shields Avenue

University of California Davis

Davis, CA 95616

530-752-3633

scdawson@ucdavis.edu

Abstract

Giardia is a common protistan parasite that causes diarrheal disease worldwide. Motile trophozoites colonize the small intestine, attaching to the villi with the ventral disc, a complex microtubule (MT) organelle. Attachment is required for infection as it allows *Giardia* to resist peristalsis. Parallel, uniformly spaced MTs spiral to form a domed structure, with one overlap zone between the upper and lower portions, and the ventral groove region extending over the ventral flagella. The MT spiral is coated with novel microribbon-crossbridge protein complexes (MR-CB) that extend up to 400 nm into the cytoplasm. The highly ordered lateral crest lies outside the disc margin at the disc periphery and forms a seal in early staged of parasite attachment. The disc is a hyperstable structure in that drugs that normally affect MT dynamic instability have no effect on ventral disc microtubules and no turnover of any disc-associated protein has been reported. Here we show that much of the ventral disc structure remains intact after detergent extraction in up to 2M potassium chloride. Using a new method of disc biochemical fractionation in high salt with shot-gun proteomic analysis of the disc, we identified and confirmed 55 new disc-associated protein (DAPs), bringing the current total of DAPs to 87. While close to 30 DAPs also localize with flagella, 54 DAPs localize specifically to the disc. Most also localize to specific structural regions of the disc such as the ventral groove or disc margin. Despite our developing understanding of the complexity of ventral disc architecture, we are still in the very preliminary stages of understanding the and composition and contribution of specific structural elements in generating the forces for attachment and stability. Future genetic, biochemical, and functional analyses of DAPs will be central toward understanding not only disc architecture and assembly, but also the overall disc conformational dynamics that promote host attachment.

Introduction

Microtubules (MTs) in protists can assemble into cytoskeletal arrays that adopt shapes, functions, or regulatory mechanisms that are not seen in other organisms. The ubiquity and diversity of unique cytoskeletal organelles in microbial eukaryotes underscores the fact that cytoskeletal variation is the norm rather than the exception. Emerging microbial eukaryotic model systems offer a wealth cytoskeletal organelles and associated proteins [1]. Diverse protistan cytoskeletal structures are often composed of proteins that lack homology to proteins in other eukaryotes [2-4], and thus may be an untapped reservoir of non-canonical MT-binding proteins governing MT assembly, nucleation, or dynamics [5]. The MT based apical complex of the apicomplexan parasite *T. gondii*, for example, acts as an invasion machine to infect of host cells and is constructed from canonical tubulins, non-canonical tubulins, and novel proteins [2, 6].

Giardia is the causative agent of giardiasis; a diarrheal disease affecting human health and livestock worldwide [7]. Commonly ingested from contaminated water sources, Giardia cysts excyst into flagellated trophozoites in the proximal small intestine where they attach to the intestinal microvilli and proliferate [8]. Giardia has no known secreted toxins and the cause of diarrhea is not well understood. Attachment occurs rapidly and is a necessary process for infection as it allows the parasite to resist peristalsis and remain in the gut. The ventral disc is a highly ordered and complex spiral microtubule (MT) array [9-14]. Parallel, uniformly spaced MTs spiral approximately one and a quarter turns into a domed structure. The disc spiral array has one region of overlap, termed the overlap zone, between the upper and lower portions of the disc. The majority of ventral disc microtubules terminate with their plus ends either on the

periphery of the disc or in the overlap zone, with a small subset observed to terminate within the disc body itself (Figure 1)

Despite our developing understanding of the complexity of ventral disc architecture (REF), we are still in the very preliminary stages of understanding the and composition and contribution of specific structural elements in generating the forces for attachment and stability. The overall architecture of the disc was first described by Cheissin over 50 years ago [15], and the first 3D high-resolution architecture of the ventral disc was obtained recently using cryo-electron tomography (cryo-ET) [16]. Cryo-ET of whole isolated ventral discs with volume averaging of repetitive structural elements provided details of the cytoskeletal architecture and revealed dense protein complexes coating nearly all protofilaments of the microtubule spiral array (FIGURE 1). In sum, the entire disc contains more than 1.2 mm of tubulin forming roughly one hundred MTs that vary in length from 2 to 18 μm [17].

In a recent proteomic analysis of detergent-extracted, isolated ventral discs, over twenty new candidate DAPs were identified that specifically localize to regions of the ventral disc or lateral crest [4].

Associated with the entire length of the MT spiral are unique substructural elements – the trilaminar microribbons – that are found throughout the disc body and extend 150-400 nm dorsally into the cytoplasm [12, 13] (see FIGURE 1). The microribbons consist of two sheets of globular subunits, separated by a fibrous inner core, forming a structure about 25 nm thick [13]. Regularly spaced crossbridge structures link adjacent microribbons [12] (see FIGURE 2). In the early 1980's, Holberton successfully fractionated and identified low-molecular weight

microribbon proteins that he termed giardins [12, 13]. Like microtubules, fractionated giardins can polymerize in solution. Microribbon polymers do not resemble canonical microtubules but they can form sheets, tactoids, and ribbons. The contribution of the microribbons to ventral disc stability, conformational dynamics, or to attachment is also unknown.

Along with previously identified substructures (e.g., microribbons and crossbridges), this study also defined several new repetitive MT-associated substructures including: three *Giardia* MT-associated proteins (gMAPs 1-3) and three MT inner proteins (gMIPS 5, 7 and 8), each associated with specific protofilaments, as well as two other substructures termed sidearms and paddles. Repeating every 8 nm, the sidearms and paddles are spaced at the distance of a single alpha/beta tubulin dimer. Crossbridges repeat every 16 nm corresponding to the distance of two alpha/beta tubulin dimers (FIGURE 1). Additional structural elements are associated with the ventral disc (FIGURE 1). These include a highly ordered structure, the lateral crest, which surrounds the periphery of the ventral disc [18] and is proposed to have contractile functions

The disc is a “hyperstable” structure in that drugs that normally affect MT dynamic instability have no effect on ventral disc microtubules [19] and no turnover of any disc-associated protein has been reported [4]. MTs of the ventral display canonical 13-protofilament tubular structure yet dynamic instability has not been observed of vdMTs and no turnover of disc associated proteins (DAPs) has been observed [4, 19]. The large number of unique microtubule associated proteins and other associated structural elements decorating the disc spiral may contribute to the observed hyperstability. The apparent hyperstability of the ventral disc is likely explained by the high degree of protein decoration around the ventral disc microtubules and suggests a

possible function for both the microribbon and crossbridge structures. Several microribbon proteins have been identified and are observed to form non-MT like polymers in solution in vitro [10, 13]. Ventral disc crossbridges join together lateral microribbons and repeat every 16nm throughout the entire ventral disc body. To date, no crossbridge associated proteins have been identified, and the structure of the crossbridges has proven troublesome to define [16, 17]. These structures have been hypothesized to be contractile and vary in length, which could explain why the crossbridges are not evident via cryoET [11]

Here we further define the extent to disc structural stability and extend the number of DAPs to 87. Over 33 DAPs lack any homology to proteins in other eukaryotes and close to thirty DAPs simply contain ankyrin repeat domains. Disc-associated ankyrin repeat proteins may contribute to disc assembly or architecture, as ankyrin repeat proteins are known to mediate protein-protein interactions, protein folding, and protein stability [20]. The composition and function of prominent substructural elements like the crossbridges, sidearms, and paddles is also unknown. Further dissection of the mechanism of disc conformational dynamics will first require an understanding of the functional roles of these unique disc substructural elements.

Materials and Methods

Giardia culture and live imaging conditions

All *G. lamblia* (ATCC 50803) strains were maintained in modified TYI-S-33 medium supplemented with bovine bile and 5% adult and 5% fetal bovine serum [56] in sterile 16 ml screw-capped disposable tubes (BD Falcon), and incubated upright at 37°C without shaking. GFP-tagging vectors

were introduced into WBC6 by electroporation (roughly 20 µg DNA) as previously described [4]. Strains were maintained with antibiotic selection (50 µg/ml puromycin [4]. All strains were thawed from frozen stocks and cultured for 24 to 48 hours prior to live imaging. Prior to live imaging, trophozoites were washed three times with warmed 1X HBS to decrease autofluorescence associated with the culture medium.

C-terminal GFP tagging of candidate disc-associated proteins

All strains were constructed as previously described (Hagen et al 2011). For C-terminal GFP episomal tag: All candidate DAP PCR forward primers were designed to bind 200 bp upstream of the gene to include the Giardia native promoter and contained the sequence CACC at the 5' end to facilitate directional cloning. Blunt-ended PCR amplicons were generated by PCR using PfuTurbo Hotstart PCR Mastermix (Stratagene) with Giardia intestinalis strain WBC6 genomic DNA. The candidate DAP PCR amplicons were subsequently subcloned into the Invitrogen pENTR/D-TOPO backbone to generate Gateway entry clones. Inserts in entry clones were sequenced to confirm the identity and correct orientation of the gene. To construct DAP-GFP fusions, positive entry clones were then recombined, via LR reaction, with a 1-fragment GFP tagging E. coli/Giardia shuttle destination vector (pcGFP1F.pac) using LR Clonase II Plus (Invitrogen). LR reactions were performed using 100 ng pcGFP1F.pac and 150 ng of DAP entry clone plasmid DNA. Positive clones were screened by digestion with AscI, and bulk plasmid DNA was prepared using Qiagen's Plasmid Midi Kit. To create C-terminal GFP-tagged candidate DAP strains, Giardia intestinalis strain WBC6 was electroporated with roughly 20 mg of plasmid DNA

(above) using the GenePulserXL (BioRad) under previously described conditions. Episomal DAP-GFP constructs were maintained in transformants using antibiotic selection (50 mg/ml puromycin).

To confirm the cellular localization of novel differentially expressed genes identified in the *in vivo* transcriptome, 55 differentially expressed *Giardia* genes were GFP-tagged via our laboratory's Gateway cloning pipeline [21]. We also tagged fourteen genes that were more highly expressed in *in vitro* culture. The C-terminal GFP fusion constructs included approximately 200–250 nucleotides upstream of the gene, the gene itself in frame with GFP, and a puromycin resistance cassette [21]. The ***Giardia*** strain WBC6 was electroporated with 20 µg of GFP-fusion plasmids, and transformed strains were maintained under antibiotic selection (50 µg/ml puromycin) for at least two weeks [21].

Biochemical fractionation of the Giardia cytoskeleton

Detergent extraction of Giardia's microtubule cytoskeleton was done as previously described (Hagen et al. 2012). First, TYI-S-33 medium was decanted from one confluent 12 ml culture of trophozoites, cells were washed three times with warm 1X HBS. Cells were iced for 15 minutes in the last HBS wash, pelleted, and resuspended in 1x PHEM (60 mM PIPES, 25 mM HEPES, 10 mM EGTA, 1 mM MgCl2, pH 7.4) containing 1% Triton X-100 and 1M KCl to demembranate. This solution was transferred to an Eppendorf tube and vortexed continuously at a medium setting for 30 minutes. To prevent proteolysis, protease inhibitors (Roche) were added to the preparation. Ventral disc cytoskeletons were then pelleted by centrifugation at 1000×g for 5

minutes, and the pellets were washed two times in 1X PHEM lacking 1% Triton X-100. Sufficient extraction of cytoskeletons was confirmed by wet mount using DIC microscopy.

Cytoskeletons were fractionated as previously described (Holberton 1981, 1983, etc.) First, an aliquot of cytoskeletons in PHEM was retained as 'fraction 1.' Cytoskeletons were then pelleted, washed, and resuspended in CB buffer (10mM Tris, 1mM EDTA, pH 7.7) for 48 hours to dissolve the crossbridges. The leftover complexes were pelleted at 1000xG for 5 mins and the supernatant was retained as 'fraction 2.' Cytoskeletal complexes were washed and resuspended in MR buffer (10mM HEPES, 5mM EDTA, pH 8.7) for 48 hours to dissolve microribbons. The remaining tubulin complexes were pelleted and the supernatant was retained as 'fraction 3.' Tubulin leftovers were resuspended in 1x PHEM and retained as 'fraction 4.'

Proteomic analyses of fractions and mass spectrometry

All MS/MS samples were analyzed using X! Tandem (The GPM, thegpm.org; version X! Tandem Alanine (2017.2.1.4)). X! Tandem was set up to search the uniprotgiardiaintestinalis_Craprev database (unknown version, 14528 entries) assuming the digestion enzyme trypsin. X! Tandem was searched with a fragment ion mass tolerance of 20 PPM and a parent ion tolerance of 20 PPM. Glu->pyro-Glu of the n-terminus, ammonia-loss of the n-terminus, gln->pyro-Glu of the n-terminus, deamidated of asparagine and glutamine, oxidation of methionine and tryptophan and dioxidation of methionine and tryptophan were specified in X! Tandem as variable modifications.

Scaffold (version Scaffold_4.8.4, Proteome Software Inc., Portland, OR) was used to validate MS/MS based peptide and protein identifications. Peptide identifications were accepted if they exceeded specific database search engine thresholds. Protein identifications were accepted if they contained at least 5 identified peptides. Proteins that contained similar peptides and could not be differentiated based on MS/MS analysis alone were grouped to satisfy the principles of parsimony. Proteins sharing significant peptide evidence were grouped into clusters.

Live imaging of GFP-tagged DAP strains

Three dimensional stacks were acquired using the Metamorph image acquisition software (MDS Technologies) with a Leica DMI 6000 wide-field inverted fluorescence microscope with a PlanApo 100X, NA 1.40 oil immersion objective. Serial sections of GFP-tagged strains were acquired at 0.2 µm intervals and deconvolved using Huygens Professional deconvolution software (SVI). Two-dimensional maximum intensity projections were created from the 3D stacks for presentation.

Transmission Electron Microscopy

Cytoskeleton preps of wild type and knockdown cells were prepared as above and applied to 400 mesh formvar/carbon coated glow-discharged grids. Negative staining was performed by applying 1% phosphotungstic acid, pH 5.4 and dried by blotting without washes. For then sections, pelleted Giardia or Giardia attached to aclar hole punches were fixed for ten minutes in 4% paraformaldehyde and secondarily fixed for 1 hour in 1% osmium tetroxide. Fixative was washed three times from the cells with cold ddH2O. Dehydration follows through ascending concentrations of ethanol, 30, 50%, then incubated for 1 hour in 2% Uranyl acetate in 50% ETOH.

Dehydration was completed through 70%, 95% x 3, ending with three changes in 100% ETOH for a minimum of 10 minutes each change. Cell were embedded in 1:1 epoxy resin:acetone overnight at room temperature. The next day the resin was removed and replaced with 100% 2x's for 2 hrs each. The aclar discs were placed at the bottom of a flat bottom beam capsule with the cells facing up and the capsule was filled with fresh resin. The blocks were polymerized at 70C overnight. The blocks were trimmed and thin sections were cut with a Leica UCT ultramicrotome (Leica Ultracut UCT, Leica, Vienna, Austria) and stained with uranyl acetate and lead citrate before viewing in the Talos L120C electron microscope (FEI/TheromoScientific Company, Hillsboro, OR., U.S.A. made in Eindhoven, The Netherlands) at 100KV. Images were acquired using the fully integrated Ceta CMOS camera.

Results

Revised cytoskeletal fractionation of ventral disc

To identify key structural features of the ventral disc and uncover new DAPs, we adapted a biochemical fractionation protocol and performed mass spectrometry on two fractions [10, 11, 22, 23]. *In vitro* isolated ventral discs are stable in PHEM buffer for weeks. To break apart this stable structure, a step-wise fractionation can be performed in which the crossbridges and other proteins are first dissolved using a chaotropic TRIS solution (fraction 2, Figure 2). Fraction 2 contained our top structural candidates because dissolution of these proteins causes significant changes to the ventral disc ultrastructure, including opening of the normally closed ventral disc spiral and separation of microtubule/microribbon pairs from their lateral counterparts. The

microtubules in these destabilized ventral discs retain some degree of curvature, likely because microribbons remain attached to the microtubules [13, 22]. We verified the dissolution of crossbridges in fraction 2 using electron microscopy (Figure 2). Microribbons are then dissolved by alternating to a high pH HEPES solution (fraction 3). Consistent with observations from other labs, flagellar components are the predominate leftovers after MR dissolution. We performed mass spectrometry on two independent extractions of fractions 2 and 3 and subtracted the proteins identified in fraction 3 from those identified in fraction 2 in order to narrow down our structural candidate list (Table 1).

Mass spectrometry of fractions

One hundred and five proteins were identified with at least five hits in fraction 2 or fraction 3 after mass spectrometry. Of these, 61 proteins are GFP tagged and 26 have verified ventral disc localization. Highly abundant cytoskeletal proteins were identified in every fraction sampled (tubulin, MBP, delta giardin, etc.). Proteins enriched in the microribbon fraction were always identified in the crossbridge fraction, likely due to the intimate relationship these structures share. Consistent with previously published data, known microribbon proteins delta giardin, Salp-1, beta giardin and gamma giardin were found in the microribbon fraction.

Sixty-two proteins were found to be exclusively enriched in fraction 2 compared to fraction 3. Of these, thirteen proteins displayed ventral disc localization (Figure 4,5). Fraction 2 contains other structures associated with the Giardia cytoskeleton including the lateral crest that surrounds the perimeter of the ventral disc, the basal bodies, and the funis. Thus, fraction 2 is not limited to only crossbridge proteins, but likely contains crossbridge proteins in solution. We predicted that

specific crossbridge proteins would be critical to maintaining the ventral disc ultrastructure because when the crossbridges are dissolved *in vitro*, the ventral disc falls apart (Figure 2) [22]. Gene knockdown candidates were prioritized based on two criteria: 1) proteins found exclusively in the crossbridge fraction, and 2) proteins that localized to the ventral disc body. Seven proteins met both stipulations (Figure 4). An additional six proteins were found exclusively in fraction 2, however these proteins displayed disc rim localization. DAP_13981 was previously determined to be a lateral crest component via immunogold EM. Other outer disc proteins may be components of the lateral crest [4].

The disc is primarily composed of proteins lacking known MT-binding properties

GFP tagging of candidates from each fraction uncovered 55 new DAPs, bringing the total number of known DAPs to eighty-seven (Figure 3). The majority of these proteins contain no predicted homology to known proteins [24]. The next most populated group contains Ankyrin repeats (29) followed by NEK kinases (13). We predict that many of these hypothetical and Ankyrin-containing proteins are structural components of the ventral disc that contribute to ventral disc stability.

In a recent proteomic analysis of detergent-extracted, isolated ventral discs, over twenty new candidate DAPs were identified that specifically localize to regions of the ventral disc or lateral crest [4]. In an ongoing GFP tagging project associated with the GiardiaDB [25], the number of DAPs has increased to closer to ninety (see TABLE 1). Like gamma-giardin [26], twenty-six DAPs lack any homology to proteins in other eukaryotes. One non-homologous DAP, median body protein (MBP, DAP16343), is associated with the disc spiral MT array, particularly with the overlap zone. MBP has been shown to be necessary for proper ventral disc biogenesis and

function [27]. Close to thirty DAPs simply contain ankyrin repeat domains. Disc-associated ankyrin repeat proteins may contribute to disc assembly or architecture, as ankyrin repeat proteins are known to mediate protein-protein interactions, protein folding, and protein stability [20].

Some DAPs share homology with members of conserved protein families, including: three members of the striated fiber (SF)–assemblins **(**beta-giardin, delta-giardin, and SALP-1 [28]); four annexin family members (e.g., alpha-giardins [29-32]), and at least twelve NEK kinases (TABLE 1). The SF-assemblin homologs beta-giardin, delta-giardin, and SALP-1 [28] likely form the structural basis of the microribbons upon which other microribbon-associated proteins assemble [18] (see TABLE 1). Beta-giardin does not turn over following photobleaching, consistent with the hyperstable state of disc microtubules [21]. *Giardia* has an expanded repertoire of over 70 NEK kinases [33], and NEK kinases have been associated with the cytoskeleton in other eukaryotes [34]. Nine of the twelve disc-associated NEKs are putative pseudokinases that lack conserved catalytic residues, however may still retain kinase activity [4].

Despite the fact that many well-known MAPs (EB1, XMAP215, and katanin) and motors (kinesins and dyneins) are present in the *Giardia* genome [35], these proteins localize to the *Giardia* flagella or spindle, but not to the ventral disc (TABLE 1). Of the over eighty DAPs identified to date, only DAP5374, a CAP-Gly protein, has a conserved microtubule binding motif [36] and thus could interact with tubulin monomers, dimers, and MT lattices. Only one of the twenty-four *Giardia* kinesins – kinesin-6a (DAP102455) – localizes to the ventral disc, in the disc margin region. DAP16263, a homolog of DIP13, also localizes to the disc. DIP13 belongs to a MT-associated

protein family conserved in diverse protists, plants, and animals that have flagellated cell stages [37, 38]. DIP13 homologs contain a conserved "KREE" binding motif that directly binds MTs [37]; however, the *Giardia* DIP13 homolog lacks this motif. In *Chlamydomonas,* DIP13 localizes to the centrioles and to cytoplasmic and flagellar MTs, and may stabilize or connect MTs to other cellular structures [37].

DAPs are primarily uncharacterized with respect to their microtubule binding or biochemical properties. Many known DAPs are likely components of the disc substructures (e.g., microribbons, crossbridges, sidearms, or paddles), whereas other DAPs may directly influence ventral disc MT dynamics including MT nucleation, MT + end binding, MT stability, and MT curvature and structure. DAPs likely generate and stabilize the curved spiral array of the ventral disc microtubules [16, 17]. Furthermore, DAPs may be required for the overall disc conformational dynamics and domed shape hypothesized to be necessary for parasite attachment [27]. Whether conserved MAPs play a role in ventral disc biogenesis or whether ventral disc biogenesis is governed by novel DAPs must also be determined. Given a high-resolution structure and a growing list of upwards of ninety disc proteins, the next steps in understanding the functioning of the ventral disc should include assigning disc proteins to the various substructures [17].

Regional variation in the structure and composition of the ventral disc

Recently, Brown et al. [17] defined specific regional variations in the ventral disc architecture that, in concert with subcellular localization of DAPs [4], articulate distinct structural regions of the ventral disc (FIGURE 1). These variations include differences in the size and spacing of the

substructures, as well as variations in protein densities within individual substructures. For example, microribbons vary in height (from 55 to about 120 nm) and their angles relative to microtubules change throughout the disc architecture [17]. Microribbons are entirely absent in the dense bands and are partially formed in the supernumerary MT array. The lateral packing of microtubule–microribbon complexes also varies substantially (about 25 nm spacing in the dense bands to about 80 nm in the disc body), and lateral packing distance may be governed by crossbridge extension or contraction [17] [12]. At the disc margin, microtubule–microribbon complexes may function as outer, laterally contractile lids that aid the disc in clamping onto the intestinal microvilli [17]. In the ventral groove region, located at the posterior of the disc, disc MTs lose much of their curvature [17]. Due to regional variations, a single microtubule can be coated with different protein densities in different disc regions, beginning at the dense band nucleation zone and terminating at the disc margin (FIGURE 1). The structural variation in the disc defined by cryo-ET is consistent with the distinct localization patterns of DAPs observed in our GFP screen. These localizations delineate the disc body (43 DAPs), the disc margin or lateral crest (43 DAPs), the overlap zone (26 DAPs), the ventral groove (18 DAPs), and the dense bands or supernumerary MTs (15 DAPs) (see FIGURE 1 and TABLE 1).

Discussion

Given the finite and relatively small number of known proteins that regulate microtubule dynamics and assembly, how do diverse eukaryotic cells create elaborate microtubule structures? We are at the very early stages of understanding the principles governing the extreme variation in cytoskeletal organelle assembly and function. The complex architecture and

functional abilities of the ventral disc challenges our conceptions of the capabilities of cytoskeletal polymers. At least with respect to the *Giardia* ventral disc, the intricate architecture is primarily composed of novel, non-homologous proteins. The function and mechanism by which regional variation in disc proteins is generated is unknown; however, the invention of novel microtubule binding or nucleation properties may facilitate the assembly of microtubule polymers into unique arrays and organelles with new functions. In this fascinating emerging model system, the ongoing development of molecular genetic and biochemical tools [19, 39, 40] will be central toward understanding not only disc architecture and assembly, but also the overall disc conformational dynamics that promote attachment to the host. How has Giardia modified conserved tubulins to form the Giardia-specific ventral disc attachment organelle? With this work, eighty-seven DAPs have now been identified, most of which share little to no homology with any known protein. The novelty of these proteins likely contributes to the manipulation of microtubule structure and behavior. In addition to Giardia-specific hypothetical proteins, many DAPs contain ankyrin repeat domains or NEK kinase domains, suggesting the importance of these particular domains to ventral disc formation and function.

Previous work has noted the importance of the crossbridges to ventral disc stability. Holberton and Ward observed that triton extracted ventral discs would lose their crossbridges over time [22]. When enough of the crossbridges disappeared, they saw unwinding of the ventral disc, especially at the ventral groove region. Despite these structural changes, the microtubules remained largely curved suggesting that the curved nature of ventral disc microtubules may be controlled by the microribbons. Consistently, our cytoskeletal preps lose nearly all of their crossbridges into fraction 2, yet curvature of the microtubule/microribbon structure remains

(Figure 2). Holberton argues that mild dissolution of CBs results in a flat disc that is more energetically stable with fully extended CBs, and that outer ventral disc structures may help to hold the lattice in the spiral conformation. Our lab has observed that the ability of the ventral disc to form a dome is crucial for functional attachment of Giardia to surfaces [27]. Therefore, the crossbridges may be critical for both structure and function of the ventral disc.

Recent studies reveal the interaction between ankyrin proteins and the microtubule cytoskeleton in diverse eukaryotes. The apicomplexan parasite, Toxoplasma gondii, uses a complex microtubule-based organelle termed the conoid for host cell invasion. The conoid is analogous to the ventral disc in that this stable microtubule structure largely contains non-conserved hypothetical proteins. Recently, Ankyrin-repeat containing proteins have been found to be crucial for structural integrity and function of the conoid [41]. In humans, Ankyrin proteins have been recognized to serve crucial roles in erythrocytes, muscles, and neurons, where they help stabilize subsets of microtubules [42]. Furthermore, ankyrins are known to interact directly with tubulins in vitro [43, 44]. These works emphasize the adaptability of Ankyrin repeat domains to facilitate microtubule processes and stabilize microtubule arrays. Consistently, truncation of Ankyrin repeat domains from both DAP_5188 and DAP_7268 affects localization of these proteins within the ventral disc. Because of their propensity for protein/protein interactions, as well as their expansion in the Giardia genome, Ankyrin repeat proteins are candidates for helping us understand evolution of the ventral disc. The expansion and variation of Ankyrin repeat proteins could serve as adapters to augment microtubule behavior, contributing to ventral disc biogenesis.

The complex ventral disc spiral MT array and associated structures (e.g., lateral crest) have evolved only in *Giardia* species. Complex cytoskeletal organelles like the disc could evolve by cooption, modification and elaboration of existing proteins or structures like flagella, or through the invention of new MT-binding proteins or other components. The sheer number of non-homologous proteins in the disc suggests that much of the complexity of the ventral disc has evolved through the invention of novel cytoskeletal proteins. The microribbon component of the ventral disc may be derived from ancestral flagellar structures as SF-assemblins are known to be associated with flagellar root structures in other protists [45] including the *Toxoplasma* apical complex [46].

Novel protein complexes define the intricate cup-shaped architecture of the ventral disc

How does a microtubule structure lacking dynamic instability generate attachment forces? While the exogenous addition of ATP to isolated *Giardia* cytoskeletons is sufficient to drive flagellar beating, exogenous addition of ATP does not result in disc conformational dynamics [22]. Suction-based forces could theoretically be generated directly via an overall conformational change of the ventral disc from a flattened to a domed shape, resulting in a negative pressure differential relative to the outside medium [27]. If the disc substructures (e.g., microribbons, crossbridges, sidearms) are flexible, subtle substructure movements could be sufficient to generate the conformational changes required for the initiation and maintenance of attachment in the absence of canonical MT dynamics (FIGURE 3). For example, knockdown of MBP (DAP16343) results in cells with an open and flattened ventral disc conformation that are unable to proceed to later stages of attachment, supporting the notion that early disc conformational

changes generate a negative pressure differential underneath the disc [47]. MBP associates specifically with the disc body, disc margin and overlap zone, as well as the median body, and the aberrant disc conformations observed after MBP knockdown are presumably the result of MBP depletion during disc biogenesis. A dome-shaped disc might also be required for proper lateral crest seal formation [48] in early stages of attachment.

Cytoskeletal innovations in protists expand the range of microtubule polymer functions

Paradigms of microtubule function, dynamics, assembly, and nucleation have been shaped by the study of the dynamic mitotic spindle and cilium in model systems. Cell biological models tend toward macroscopic eukaryotes, yet microbial eukaryotes, or protists, have a myriad of unique interphase cytoskeletal organelles that have been described for nearly 300 years [49]. Non-canonical cytoskeletal arrays confer unique and adaptive functions to eukaryotic cells – expanding the known functional capacities of microtubule polymers and challenging conventional notions of microtubule organellar dynamics.

Materials and Methods

Giardia Culture

Giardia intestinalis strain WBC6 (ATCC 50803) trophozoites were maintained at 37°C in modified TYI-S_33 medium with bovine bile (26) in 16-ml screw-cap tubes (Fisher Scientific). Upon reaching confluency, the strain was split by first placing tubes on ice for 15 minutes then

transferring 0.5ml of detached culture to 11.5ml of warmed media. Prior to imaging, cells were washed 3x with warm 1xHBS to remove autofluorescence associated with culture media.

Giardia GFP-tagged Strain Generation

All strains were constructed as previously described (Hagen et al 2011). For C-terminal GFP episomal tag: All candidate DAP PCR forward primers were designed to bind 200 bp upstream of the gene to include the Giardia native promoter and contained the sequence CACC at the 5' end to facilitate directional cloning. Blunt-ended PCR amplicons were generated by PCR using PfuTurbo Hotstart PCR Mastermix (Stratagene) with Giardia intestinalis strain WBC6 genomic DNA. The candidate DAP PCR amplicons were subsequently subcloned into the Invitrogen pENTR/D-TOPO backbone to generate Gateway entry clones. Inserts in entry clones were sequenced to confirm the identity and correct orientation of the gene. To construct DAP-GFP fusions, positive entry clones were then recombined, via LR reaction, with a 1-fragment GFP tagging E. coli/Giardia shuttle destination vector (pcGFP1F.pac) using LR Clonase II Plus (Invitrogen). LR reactions were performed using 100 ng pcGFP1F.pac and 150 ng of DAP entry clone plasmid DNA. Positive clones were screened by digestion with AscI, and bulk plasmid DNA was prepared using Qiagen's Plasmid Midi Kit. To create C-terminal GFP-tagged candidate DAP strains, Giardia intestinalis strain WBC6 was electroporated with roughly 20 mg of plasmid DNA (above) using the GenePulserXL (BioRad) under previously described conditions. Episomal DAP-GFP constructs were maintained in transformants using antibiotic selection (50 mg/ml puromycin).

Biochemical Fractionation

Detergent extraction of Giardia's microtubule cytoskeleton was done as previously described (Hagen et al. 2012). First, TYI-S-33 medium was decanted from one confluent 12 ml culture of trophozoites, cells were washed three times with warm 1X HBS. Cells were iced for 15 minutes in the last HBS wash, pelleted, and resuspended in 1x PHEM (60 mM PIPES, 25 mM HEPES, 10 mM EGTA, 1 mM MgCl2, pH 7.4) containing 1% Triton X-100 and 1M KCl to demembranate. This solution was transferred to an Eppendorf tube and vortexed continuously at a medium setting for 30 minutes. To prevent proteolysis, protease inhibitors (Roche) were added to the preparation. Ventral disc cytoskeletons were then pelleted by centrifugation at 1000×g for 5 minutes, and the pellets were washed two times in 1X PHEM lacking 1% Triton X-100. Sufficient extraction of cytoskeletons was confirmed by wet mount using DIC microscopy.

Cytoskeletons were fractionated as previously described (Holberton 1981, 1983, etc.) First, an aliquot of cytoskeletons in PHEM was retained as 'fraction 1.' Cytoskeletons were then pelleted, washed, and resuspended in CB buffer (10mM Tris, 1mM EDTA, pH 7.7) for 48 hours to dissolve the crossbridges. The leftover complexes were pelleted at 1000xG for 5 mins and the supernatant was retained as 'fraction 2.' Cytoskeletal complexes were washed and resuspended in MR buffer (10mM HEPES, 5mM EDTA, pH 8.7) for 48 hours to dissolve microribbons. The remaining tubulin complexes were pelleted, and the supernatant was retained as 'fraction 3.' Tubulin leftovers were resuspended in 1x PHEM and retained as 'fraction 4.'

Mass Spectrometry

All MS/MS samples were analyzed using X! Tandem (The GPM, thegpm.org; version X! Tandem Alanine (2017.2.1.4)). X! Tandem was set up to search the uniprot giardiaintestinalis_Craprev

database (unknown version, 14528 entries) assuming the digestion enzyme trypsin. X! Tandem was searched with a fragment ion mass tolerance of 20 PPM and a parent ion tolerance of 20 PPM. Glu->pyro-Glu of the n-terminus, ammonia-loss of the n-terminus, gln->pyro-Glu of the n-terminus, deamidated of asparagine and glutamine, oxidation of methionine and tryptophan and dioxidation of methionine and tryptophan were specified in X! Tandem as variable modifications.

Scaffold (version Scaffold_4.8.4, Proteome Software Inc., Portland, OR) was used to validate MS/MS based peptide and protein identifications. Peptide identifications were accepted if they exceeded specific database search engine thresholds. Protein identifications were accepted if they contained at least 5 identified peptides. Proteins that contained similar peptides and could not be differentiated based on MS/MS analysis alone were grouped to satisfy the principles of parsimony. Proteins sharing significant peptide evidence were grouped into clusters.

Confocal Microscopy

3D stacks and time lapse movies were acquired of live cells grown in 96-well #1.5 black glass bottom imaging plates (In Vitro Scientific). Images were acquired with the spinning-disk module of a Marianas SDC Real-Time 3D Confocal-TIRF microscope (Intelligent Imaging Innovations) fit with a Yokogawa spinning-disk head, a 63×/1.3 NA oil-immersion objective, and electron-multiplying charge-coupled device camera. Acquisition was controlled by SlideBook 6 software (3i Incorporated). All raw images were exposed and scaled with the same parameters.

Transmission Electron Microscopy

Cytoskeleton preps of wild type and knockdown cells were prepared as above and applied to 400 mesh formvar/carbon coated glow-discharged grids. Negative staining was performed by applying 1% phosphotungstic acid, pH 5.4 and dried by blotting without washes. For then sections, pelleted Giardia or Giardia attached to aclar hole punches were fixed for ten minutes in 4% paraformaldehyde and secondarily fixed for 1 hour in 1% osmium tetroxide. Fixative was washed three times from the cells with cold ddH2O. Dehydration follows through ascending concentrations of ethanol, 30, 50%, then incubated for 1 hour in 2% Uranyl acetate in 50% ETOH. Dehydration was completed through 70%, 95% x 3, ending with three changes in 100% ETOH for a minimum of 10 minutes each change. Cell were embedded in 1:1 epoxy resin:acetone overnight at room temperature. The next day the resin was removed and replaced with 100% 2x's for 2 hrs each. The aclar discs were placed at the bottom of a flat bottom beam capsule with the cells facing up and the capsule was filled with fresh resin. The blocks were polymerized at 70C overnight. The blocks were trimmed, and thin sections were cut with a Leica UCT ultramicrotome (Leica Ultracut UCT, Leica, Vienna, Austria) and stained with uranyl acetate and lead citrate before viewing in the Talos L120C electron microscope (FEI/TheromoScientific Company, Hillsboro, OR., U.S.A. made in Eindhoven, The Netherlands) at 100KV. Images were acquired using the fully integrated Ceta CMOS camera.

Acknowledgements

Thank you to Michael Paddy of the UC Davis MCB Microscopy Core with helpful advice on SDC and SIM microscopes. Thank you to Patricia Kysar of the UC Davis MCB Electron Microscopy Lab for advice and training on TEM. Thank you to Michelle Salemi and Brett Phinney at the UCD

Proteomics Core for help with mass spectroscopy. Kari Hagen and Shane McInally provided helpful readings of manuscript drafts.

Figure legends

Figure 1. Ventral disc substructures support the microtubule array. A schematic of the ventral disc indicated the primary structure elements is shown in panel A: OZ: overlap zone, BB: basal bodies, LC: lateral crest, VG: ventral groove, FU: funis (A), MT: microtubule, MR: microribbon, CB: crossbridge (B,C). In B, a negative-stained cytoskeletal preparation of the ventral disc In C, TEM of thin sections from whole embedded *Giardia* trophozoites show both microribbons (MR) crossbridges (CB) complexes associated with the entire microtubule (MT) spiral organelle (D). A seciton of the lateral crest (LC) is on the edge of disc (C). In E, the overlap zone (OZ) of the MT spiral array, along with the MR-CB complexes are seen in cross section.

Figure 2. Prominent disc structural elements are hyperstable. Ventral disc structure is insensitive to MT stabilizing or depolymerizing drugs such as taxol or nocodazole (A), yet flagella and median body are dynamic and sensitive to drugs (B). Much of ventral disc structural elements such as microribbons and microtubules remain intact following extraction in up to 2M KCl (C), and tagged microribbon (delta giardin), overlap zone (MBP) proteins remain associated with the disc microtubule array even after extraction with 2M KCl.

Figure 3: Sequential fractionation of ventral disc substructures. Cartoon depicts ventral disc fractionation (A). First, membrane and cytosol are removed from the *Giardia* microtubule cytoskeleton (P1) in panels B, and negative stain electron microscopy image in D. Panel C shows a representation tubulin (purple) and delta-giardin (green) immunostained cytoskeleton from P1 fraction. Next, crossbridges and other proteins are removed, destabilizing the ventral disc (P3) in E, and tubulin-stained image of dissociated discs in F. SDS-PAGE indicates different proteins

that are enriched in each pellet and supernatant (G) and in the Venn Diagram comparisons of mass spectrometry of fractions (E).

Figure 4. Many of the 87 disc associated proteins (DAPs) localize to other cytoskeletal structures. Localizations were categorized into those associated localizing exclusively to the disc (disc only, N=42), or also to the flagella (including the basal bodies, cytoplasmic axonemes and membrane bound regions of the eight flagella (N=31), as well as the median body(N=12), lateral crest (N=4) are presented as in the Venn diagram comparisons. Representative localizations are also shown for each of the categories of localizations for the GFP tagged DAP strains.

Figure 5. Disc-associated proteins localize to specific structurally distinct regions of the ventral disc. The 54 disc (and median body-localizing) DAPs were compared with respect to localization to the disc MT spiral array (disc body), disc margin (DM), ventral groove (VG), dense bands (DB), and overlap zone (OZ). Representative DAPs are presented to demonstrate the number and type of regional localization categories presented in the Venn Diagram.

Bibliography

1. Russell, J.J., et al., *Non-model model organisms.* BMC Biol, 2017. **15**(1): p. 55.
2. Hu, K., et al., *Cytoskeletal components of an invasion machine--the apical complex of Toxoplasma gondii.* PLoS Pathog, 2006. **2**(2): p. e13.
3. Preisner, H., et al., *The Cytoskeleton of Parabasalian Parasites Comprises Proteins that Share Properties Common to Intermediate Filament Proteins.* Protist, 2016. **167**(6): p. 526-543.
4. Hagen, K.D., et al., *Novel structural components of the ventral disc and lateral crest in Giardia intestinalis.* PLoS Negl Trop Dis, 2011. **5**(12): p. e1442.
5. Hampl, V., et al., *Phylogenomic analyses support the monophyly of Excavata and resolve relationships among eukaryotic "supergroups".* Proc Natl Acad Sci U S A, 2009. **106**(10): p. 3859-64.
6. Morrissette, N., *Targeting Toxoplasma tubules: tubulin, microtubules, and associated proteins in a human pathogen.* Eukaryot Cell, 2015. **14**(1): p. 2-12.
7. Einarsson, E., S. Ma'ayeh, and S.G. Svard, *An up-date on Giardia and giardiasis.* Curr Opin Microbiol, 2016. **34**: p. 47-52.
8. Nosala, C. and S.C. Dawson, *The Critical Role of the Cytoskeleton in the Pathogenesis of Giardia.* Curr Clin Microbiol Rep, 2015. **2**(4): p. 155-162.
9. Feely, D.E., J.V. Schollmeyer, and S.L. Erlandsen, *Giardia spp.: distribution of contractile proteins in the attachment organelle.* Exp Parasitol, 1982. **53**(1): p. 145-54.
10. Crossley, R. and D.V. Holberton, *Assembly of 2.5 nm filaments from giardin, a protein associated with cytoskeletal microtubules in Giardia.* J Cell Sci, 1985. **78**: p. 205-31.

11. Crossley, R. and D.V. Holberton, *Characterization of proteins from the cytoskeleton of Giardia lamblia.* J Cell Sci, 1983. **59**: p. 81-103.

12. Holberton, D.V., *Fine structure of the ventral disk apparatus and the mechanism of attachment in the flagellate Giardia muris.* J Cell Sci, 1973. **13**(1): p. 11-41.

13. Holberton, D.V., *Arrangement of subunits in microribbons from Giardia.* J Cell Sci, 1981. **47**: p. 167-85.

14. Friend, D.S., *The fine structure of Giardia muris.* J Cell Biol, 1966. **29**(2): p. 317-32.

15. Cheissin, E.M., *Ultrastructure of Lamblia Duodenalis. I. Body Surface, Sucking Disc and Median Bodies.* J Protozool, 1964. **11**: p. 91-8.

16. Schwartz, C.L., et al., *A detailed, hierarchical study of Giardia lamblia's ventral disc reveals novel microtubule-associated protein complexes.* PLoS One, 2012. **7**(9): p. e43783.

17. Brown, J.R., et al., *A detailed look at the cytoskeletal architecture of the Giardia lamblia ventral disc.* J Struct Biol, 2016. **194**(1): p. 38-48.

18. Feely, D.E., Hoberton, D.V., Erlandsen, S.L., *The Biology of Giardia*, in *Giardiasis*, E.A. Meyer, Editor. 1990, Elsevier: Amsterdam. p. 11-50.

19. Dawson, S.C., et al., *Kinesin-13 regulates flagellar, interphase, and mitotic microtubule dynamics in Giardia intestinalis.* Eukaryot Cell, 2007. **6**(12): p. 2354-64.

20. Li, J., A. Mahajan, and M.D. Tsai, *Ankyrin repeat: a unique motif mediating protein-protein interactions.* Biochemistry, 2006. **45**(51): p. 15168-78.

21. Dawson, S.C. and S.A. House, *Imaging and analysis of the microtubule cytoskeleton in Giardia.* Methods Cell Biol, 2010. **97**: p. 307-39.

22. Holberton, D.V. and A.P. Ward, *Isolation of the cytoskeleton from Giardia. Tubulin and a low-molecular-weight protein associated with microribbon structures.* J Cell Sci, 1981. **47**: p. 139-66.

23. Crossley, R. and D.V. Holberton, *Selective extraction with Sarkosyl and repolymerization in vitro of cytoskeleton proteins from Giardia.* J Cell Sci, 1983. **62**: p. 419-38.

24. Nosala, C., K.D. Hagen, and S.C. Dawson, *'Disc-o-Fever': Getting Down with Giardia's Groovy Microtubule Organelle.* Trends Cell Biol, 2018. **28**(2): p. 99-112.

25. Aurrecoechea, C., et al., *GiardiaDB and TrichDB: integrated genomic resources for the eukaryotic protist pathogens Giardia lamblia and Trichomonas vaginalis.* Nucleic Acids Res, 2009. **37**(Database issue): p. D526-30.

26. Nohria, A., R.A. Alonso, and D.A. Peattie, *Identification and characterization of gamma giardin and the gamma giardin gene from Giardia lamblia.* Mol Biochem Parasitol, 1992. **56**(1): p. 27-37.

27. Woessner, D.J. and S.C. Dawson, *The Giardia median body protein is a ventral disc protein that is critical for maintaining a domed disc conformation during attachment.* Eukaryot Cell, 2012. **11**(3): p. 292-301.

28. Palm, J.E., et al., *Identification of immunoreactive proteins during acute human giardiasis.* J Infect Dis, 2003. **187**(12): p. 1849-59.

29. Weiland, M.E., et al., *Annexin-like alpha giardins: a new cytoskeletal gene family in Giardia lamblia.* Int J Parasitol, 2005. **35**(6): p. 617-26.

30. Weiland, M.E., et al., *Characterisation of alpha-1 giardin: an immunodominant Giardia lamblia annexin with glycosaminoglycan-binding activity.* Int J Parasitol, 2003. **33**(12): p. 1341-51.

31. Bauer, B., et al., *Functional identification of alpha 1-giardin as an annexin of Giardia lamblia.* FEMS Microbiol Lett, 1999. **173**(1): p. 147-53.

32. Peattie, D.A., *The giardins of Giardia lamblia: genes and proteins with promise.* Parasitol Today, 1990. **6**(2): p. 52-56.

33. Manning, G., et al., *The minimal kinome of Giardia lamblia illuminates early kinase evolution and unique parasite biology.* Genome biology, 2011. **12**(7): p. R66.

34. O'Regan, L., J. Blot, and A.M. Fry, *Mitotic regulation by NIMA-related kinases.* Cell Div, 2007. **2**: p. 25.

35. Morrison, H.G., et al., *Genomic minimalism in the early diverging intestinal parasite Giardia lamblia.* Science, 2007. **317**(5846): p. 1921-6.

36. Weisbrich, A., et al., *Structure-function relationship of CAP-Gly domains.* Nat Struct Mol Biol, 2007. **14**(10): p. 959-67.

37. Pfannenschmid, F., et al., *Chlamydomonas DIP13 and human NA14: a new class of proteins associated with microtubule structures is involved in cell division.* J Cell Sci, 2003. **116**(Pt 8): p. 1449-62.

38. Fritz-Laylin, L.K., et al., *The genome of Naegleria gruberi illuminates early eukaryotic versatility.* Cell, 2010. **140**(5): p. 631-42.

39. Touz, M.C., J.T. Conrad, and T.E. Nash, *A novel palmitoyl acyl transferase controls surface protein palmitoylation and cytotoxicity in Giardia lamblia.* Mol Microbiol, 2005. **58**(4): p. 999-1011.

40. Carpenter, M.L. and W.Z. Cande, *Using morpholinos for gene knockdown in Giardia intestinalis.* Eukaryot Cell, 2009. **8**(6): p. 916-9.

41. Long, S., et al., *A conserved ankyrin repeat-containing protein regulates conoid stability, motility and cell invasion in Toxoplasma gondii.* Nat Commun, 2017. **8**(1): p. 2236.

42. Goellner, B. and H. Aberle, *The synaptic cytoskeleton in development and disease.* Dev Neurobiol, 2012. **72**(1): p. 111-25.

43. Davis, J.Q. and V. Bennett, *Brain ankyrin. A membrane-associated protein with binding sites for spectrin, tubulin, and the cytoplasmic domain of the erythrocyte anion channel.* J Biol Chem, 1984. **259**(21): p. 13550-9.

44. Bennett, V. and J. Davis, *Erythrocyte ankyrin: immunoreactive analogues are associated with mitotic structures in cultured cells and with microtubules in brain.* Proc Natl Acad Sci U S A, 1981. **78**(12): p. 7550-4.

45. Weber, K., et al., *SF-assemblin, the structural protein of the 2-nm filaments from striated microtubule associated fibers of algal flagellar roots, forms a segmented coiled coil.* J Cell Biol, 1993. **121**(4): p. 837-45.

46. Francia, M.E., et al., *Cell division in Apicomplexan parasites is organized by a homolog of the striated rootlet fiber of algal flagella.* PLoS Biol, 2012. **10**(12): p. e1001444.

47. Hansen, W.R., et al., *Giardia lamblia attachment force is insensitive to surface treatments.* Eukaryot Cell, 2006. **5**(4): p. 781-3.

48. House, S.A., et al., *Giardia flagellar motility is not directly required to maintain attachment to surfaces.* PLoS Pathog, 2011. **7**(8): p. e1002167.

49. Dawson, S.C. and A.R. Paredez, *Alternative cytoskeletal landscapes: cytoskeletal novelty and evolution in basal excavate protists.* Curr Opin Cell Biol, 2013. **25**(1): p. 134-41.

1.

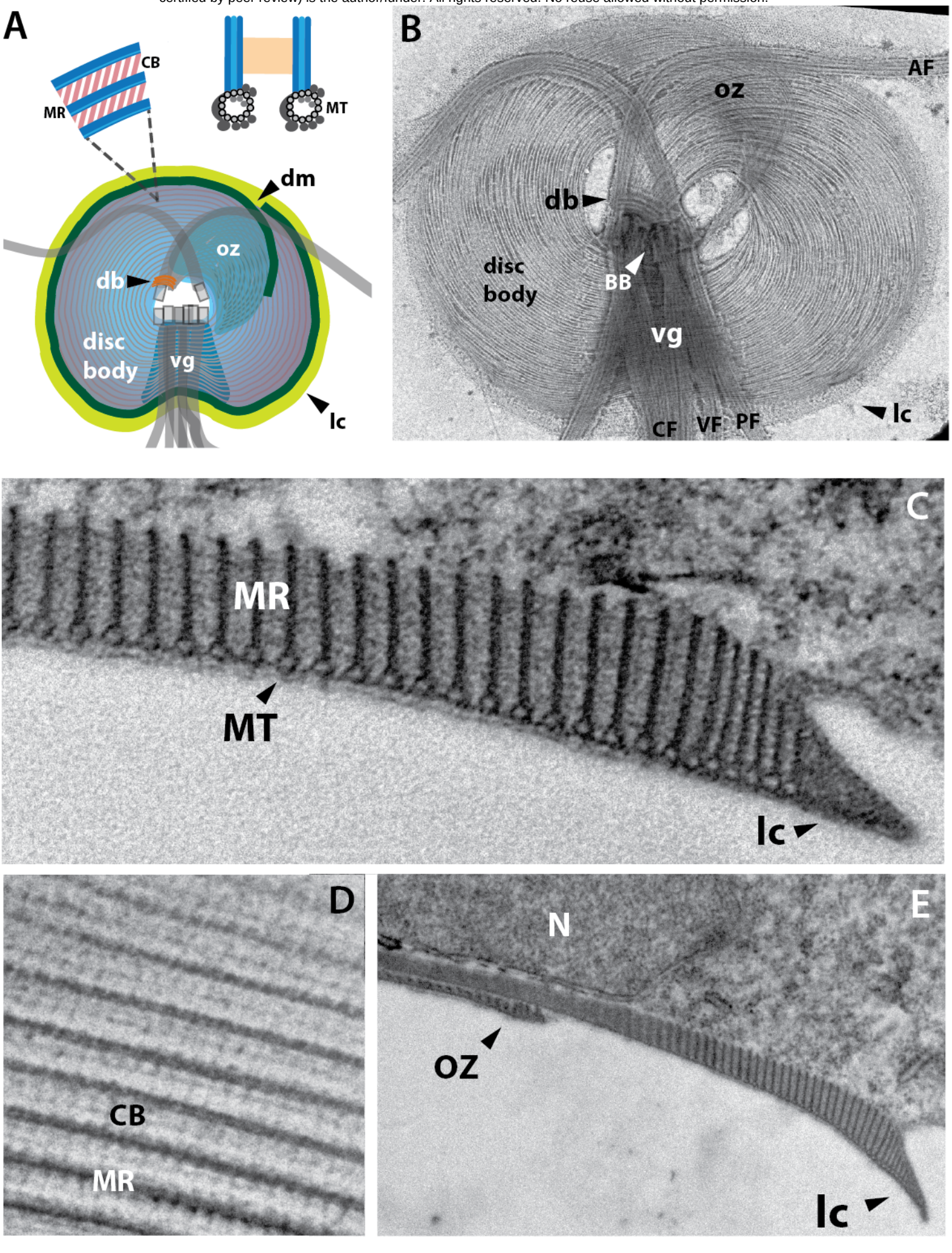

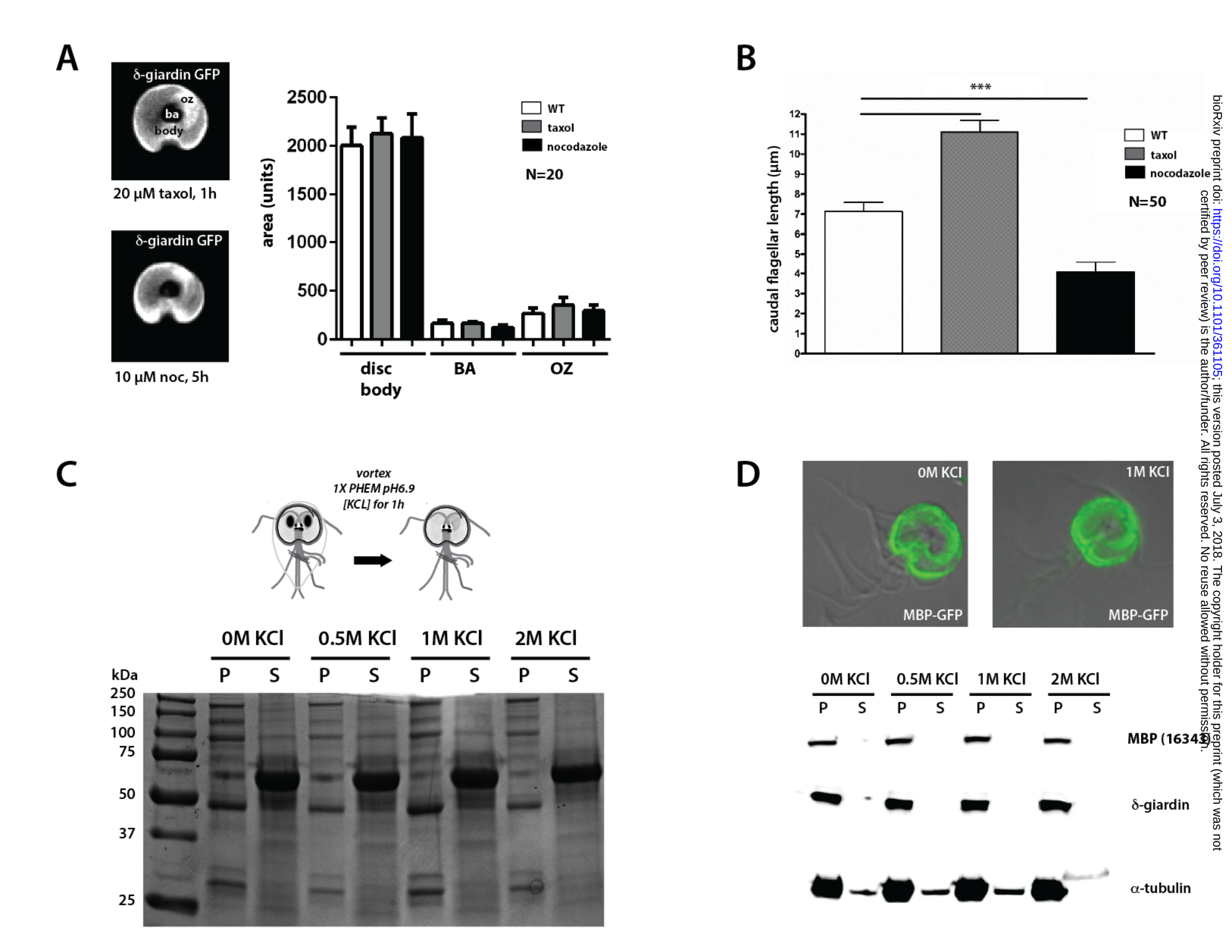

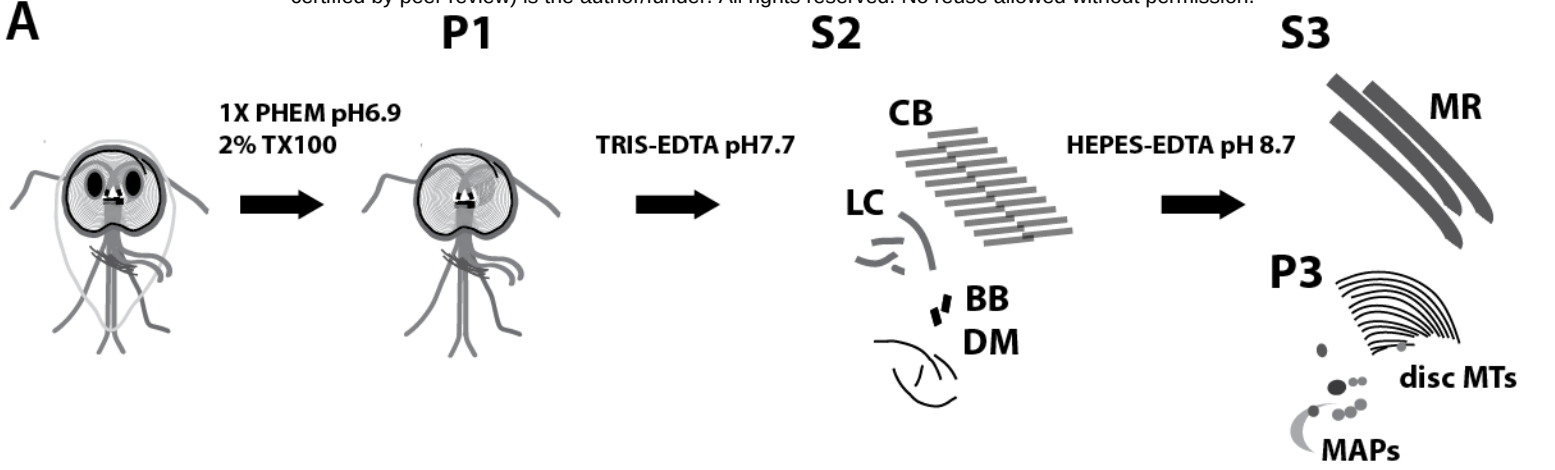

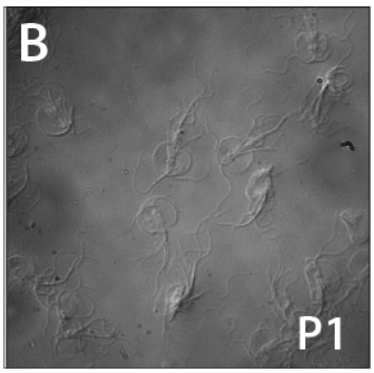

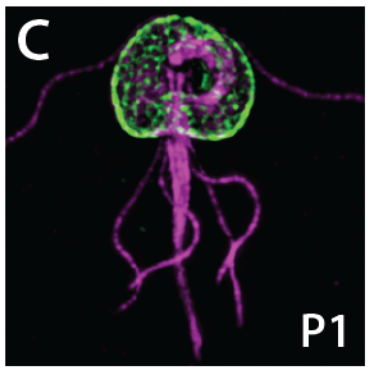

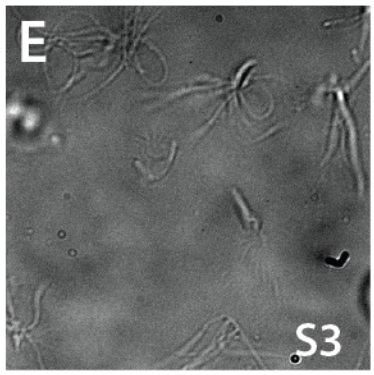

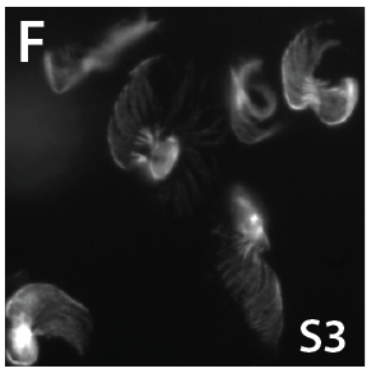

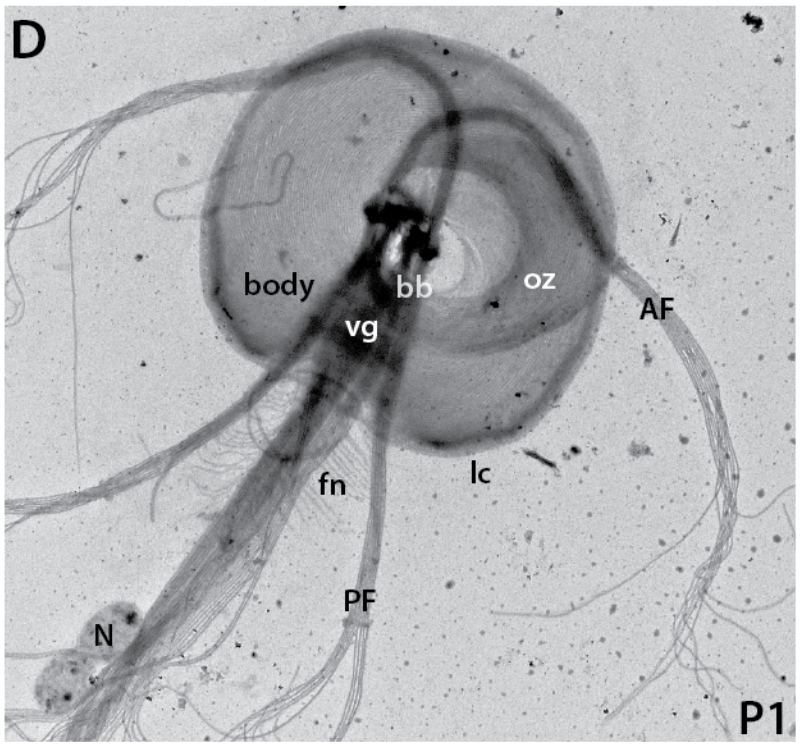

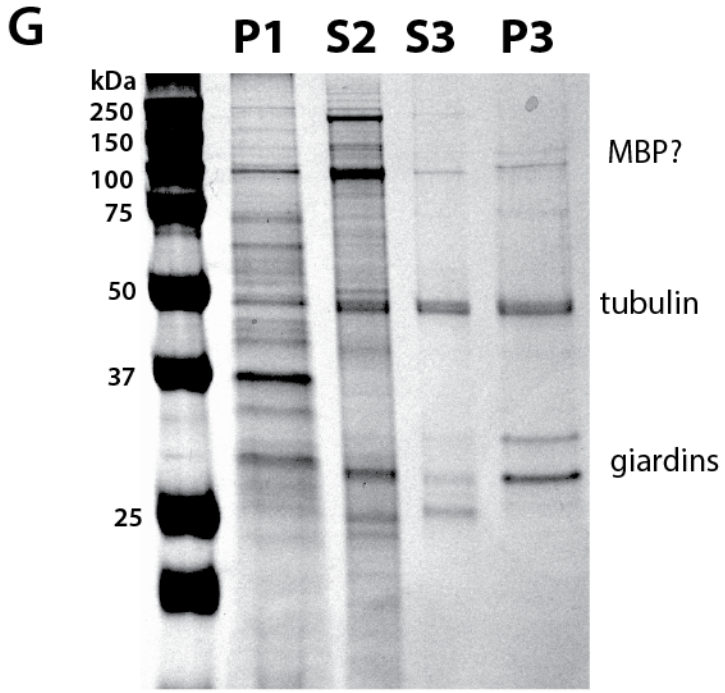

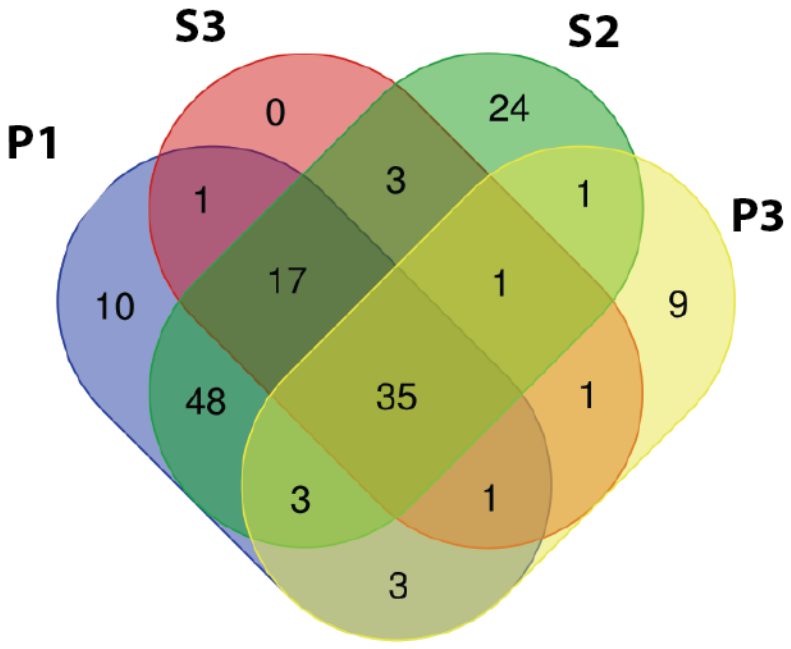

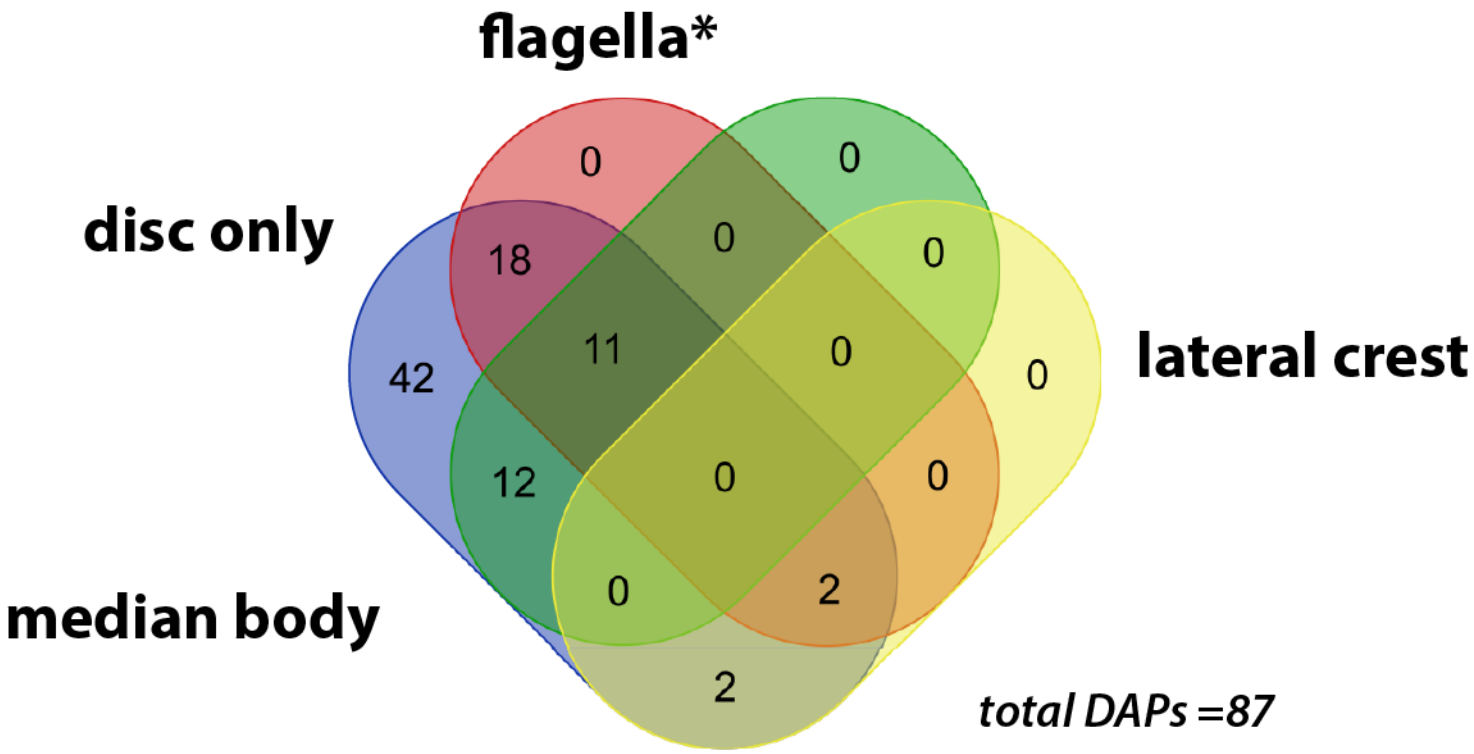

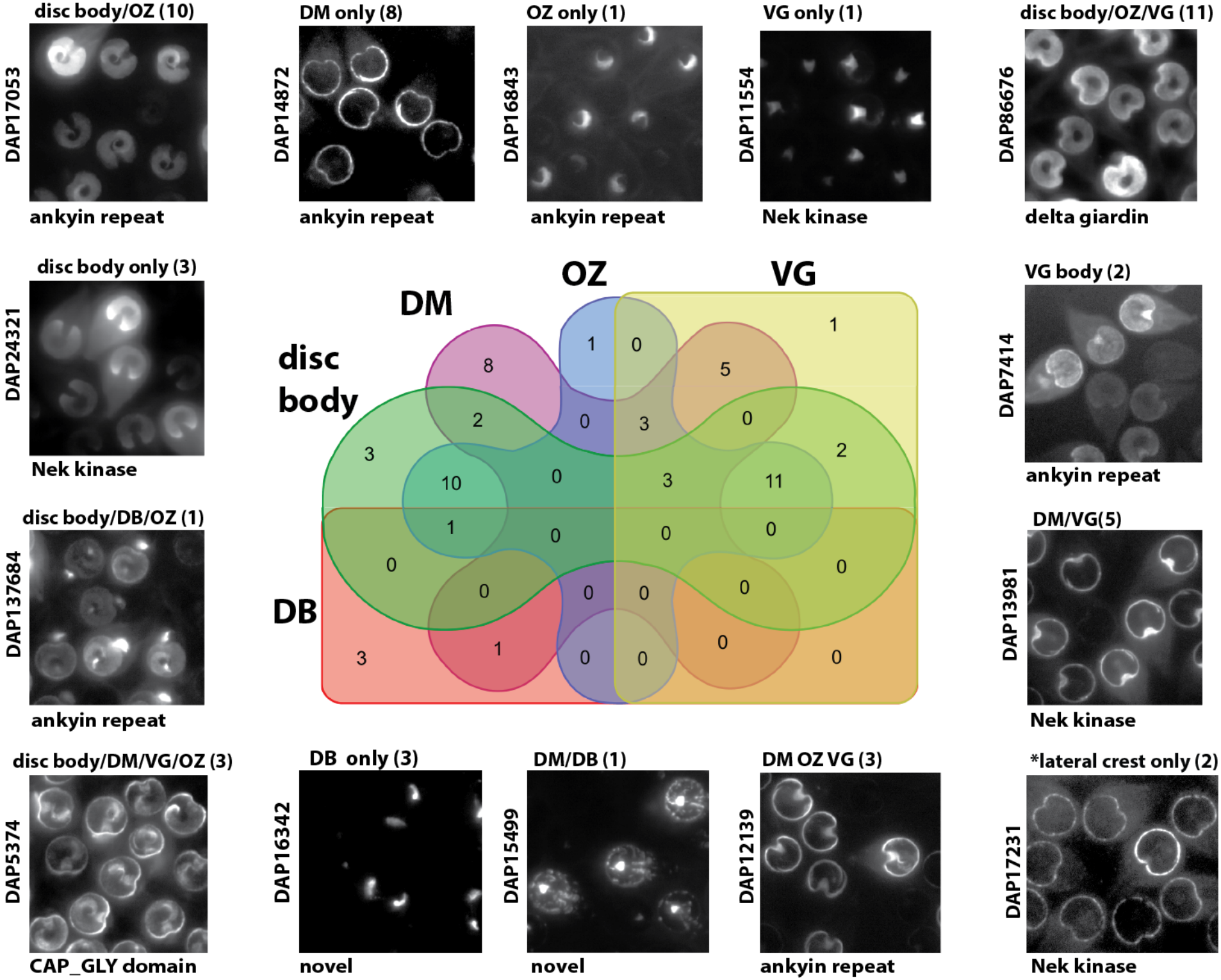

**no image disc body/DM (2)

GiardiaDB	annotation	MW (kDa)	PFAM	P1K	P1M	MR1	MR3	CB1
GL50803_4812	beta giardin	31	SF-assemblin	191	44	511	92	242
GL50803_16343	median body protein	101	none	70	31	268	58	195
GL50803_17230	gamma giardin	36	none	105	12	232	38	83
GL50803_86676	delta-giardin	34	SF-assemblin	50	7	171	48	130
GL50803_12139	ankyrin repeat protein	76	ankyrin	42	19	136	42	80
GL50803_137716	GASP-180 family protein	175	ankyrin	387	63	94	66	662
GL50803_4410	SALP-1		SF assemblin	24	1	67	34	55
GL50803_4852	hypothetical protein	49	none	13	22	67	4	19
GL50803_113622	ankyrin repeat protein	164	ankyrin	25	7	62	3	49
GL50803_14859	ankyrin repeat protein	103	ankyrin	99	45	60	6	419
GL50803_13475	GASP-180 family protein	236	ankyrin	20	21	55	26	189
GL50803_7444	hypothetical protein	41	none	31	16	55	12	79
GL50803_10524	hypothetical protein	27	none	28	8	53	7	29
GL50803_17551	ankyrin repeat protein	119	ankyrin	80	72	47	14	224
GL50803_27925	ankyrin repeat protein	88	ankyrin	153	56	44	4	376
GL50803_24537	hypothetical protein	59	none	17	11	31	21	106
GL50803_9515	ankyrin repeat protein	150	ankyrin	32	37	31	20	227
GL50803_5489	Nek kinase GK271	61	kinase	7	1	28	8	2
GL50803_5188	ankyrin repeat protein	57	ankyrin	11	9	25	7	25
GL50803_88369	ankyrin repeat protein	92	ankyrin	7	7	25	0	40
GL50803_16532	ankyrin repeat protein	93	ankyrin	46	36	23	15	141
GL50803_11165	ankyrin repeat protein	82	ankyrin	16	6	23	2	44
GL50803_16844	hypothetical protein	35	none	29	9	23	0	3
GL50803_15410	Ser/Thr protein kinase	32	ankyrin	46	11	20	12	70
GL50803_5883	hypothetical protein	63	none	32	26	19	23	118
GL50803_17468	hypothetical protein	36	none	10	10	19	4	13
GL50803_10527	hypothetical protein	35	none	2	0	17	2	14
GL50803_8726	hypothetical protein	106	none	8	19	15	26	142
GL50803_17097	ankyrin repeat protein	163	ankyrin	0	0	15		66
GL50803_15499	hypothetical protein	49	none	23	14	13	4	20
GL50803_7268	ankyrin repeat protein	126	ankyrin	8	3	13	0	5
GL50803_112557	ankyrin repeat protein	89	ankyrin	7	1	13	0	0

GL50803_41512	DUF1126 domain	74	DUF1126	20	3	11	0	0
GL50803_15409	Nek kinase GK175	57	kinase	164	23	9	21	63
GL50803_4239	hypothetical protein	11	none	4	0	8	5	34
GL50803_17046	ankyrin repeat protein	75	ankyrin	18	14	8	4	28
GL50803_16424	Mlf1IP domain protein	30	Mlf1IP	13	2	8	0	11
GL50803_13584	hypothetical protein	44	none	48	41	7	10	88
GL50803_16935	hypothetical protein	94	none	11	5	7	3	2
GL50803_6709	hypothetical protein	58	none	1	4	7	0	0
GL50803_9030	ankyrin repeat protein	37	ankyrin	48	35	6	6	92
GL50803_9148	SHIPPO repeat family protein	22	SHIPPO-repeat	7	20	6	2	13
GL50803_16720	radial spokehead family protein	96	rsp	13	0	5	2	41
GL50803_14921	hypothetical protein	55	none	11	18	5	2	6
GL50803_16996	enkurin superfamily protein	46	enkurin	8	1	5	0	7
GL50803_16279	Nek kinase GK256	75	kinase	4	1	4	0	15
GL50803_91354	SHIPPO repeat family protein	63	SHIPPO-repeat	14	31	3	5	16
GL50803_9848	dynein light chain	10	LC8	16	2	3	0	9
GL50803_13372	TPH domain protein	55	TPH	6	2	3	0	6
GL50803_11654	alpha1-giardin	34	annexin	121	11	2	13	34
GL50803_17585	ankyrin repeat protein	77	ankyrin	22	24	2	4	78
GL50803_104685	centrin	20	centrin	4	17	1	4	26
GL50803_11554	Nek kinase GK249	32	kinase	7	0	1	2	21
GL50803_16263	conserved hypothetical protein	12	none	2	6	1	0	18
GL50803_7520	hypothetical protein	54	none	2	0	1	0	41
GL50803_137684	ankyrin repeat protein		ankyrin	2	0	0		0
GL50803_101291	beta-tubulin 1	50	tubulin	503	42	0	120	0
GL50803_103676	alpha tubulin 1	51	tubulin	360	40	0	59	0
GL50803_17249	hypothetical protein	191	none	81	34	0	24	6
GL50803_41212	ankyrin repeat protein	149	ankyrin	90	33	0	23	25
GL50803_15411	Nek kinase GK292	78	kinase	83	22	0	8	7
GL50803_16745	GASP-180 family protein	116	ankyrin	117	54	0	7	21
GL50803_7796	alpha2-giardin	34	annexin	17	4	0	6	38
GL50803_17153	alpha11-giardin	35	annexin	58	6	0	6	7
GL50803_10167	hypothetical protein	133	none	42	18	0	6	0

GL50803_10808	hypothetical protein	25	none	9	0	0	6	0
GL50803_100955	mitotic spindle checkpoint MAD2	23	horma domain	5	0	0	5	0
GL50803_16521	alpha SNAP	32	SNAP	2	4	0	5	21
GL50803_17096	ankyrin repeat protein	85	ankyrin	5	5	0	2	44
GL50803_94463	hypothetical protein	53	none	27	20	0	2	42
GL50803_16648	hypothetical protein	88	none	22	5	0	2	0
GL50803_14434	ankyrin repeat protein	50	ankyrin	16	11	0	2	0
GL50803_8854	hypothetical protein	70	none	12	2	0	2	0
GL50803_15035	Nek kinase GK210	59	kinase	10	1	0	2	0
GL50803_3582	hypothetical protein	40	none	4	6	0	2	6
GL50803_13651	hypothetical protein		none	17	7	0	0	0
GL50803_10232	hypothetical protein		none	7	2	0	0	0
GL50803_33866	hypothetical protein		none	2	0	0	0	0
GL50803_16342	hypothetical protein		none	2	0	0	0	0
GL50803_5374	tubulin-specific chaperone B		CAP-GLY	0	0	0	0	0
GL50803_11683	alpha3-giardin		annexin	0	0	0	0	0
GL50803_3256	epsin		ENTH	0	0	0	0	0
GL50803_16272	Nek kinase GK187		kinase, ankyrin	0	0	0	0	0
GL50803_17412	hypothetical protein		none	0	0	0	0	0
GL50803_17563	ERK1 kinase		kinase	0	0	0	0	0
GL50803_13981	Nek kinase GK185	123	kinase, ankyrin	0	4	0	0	33
GL50803_3957	Nek kinase GK212		kinase, ankyrin	0	0	0	0	0
GL50803_6751	hypothetical protein		none	0	0	0	0	0
GL50803_24194	ankyrin repeat protein		ankyrin	3	0	0	0	0
GL50803_14872	ankyrin repeat protein	137	ankyrin	1	2	0	0	14
GL50803_103810	ankyrin repeat protein		ankyrin	0	0	0	0	0
GL50803_15576	ankyrin repeat protein		ankyrin	0	0	0	0	0
GL50803_10219	ankyrin repeat protein	159	ankyrin	8	2	0	0	14
GL50803_14800	ankyrin repeat protein		ankyrin	0	3	0	0	0
GL50803_8850	ankyrin repeat protein		ankyrin	0	0	0	0	0
GL50803_5568	DUF866 domain protein		DUF866	0	0	0	0	0
GL50803_10893	Nek kinase GK193		kinase	0	0	0	0	0
GL50803_11775	Nek kinase GK301		kinase, ankyrin	0	0	0	0	0

GL50803_103164	SHIPPO repeat family protein		SHIPPO-repeat	0	0	0	0	0
GL50803_102455	GiKIN6a		kinesin-6	0	0	0	0	0
GL50803_6171	hypothetical protein		none	0	0	0	0	0
GL50803_23492	ankyrin repeat protein		ankyrin	5	13	0	0	0
GL50803_17231	Nek kinase GK186	111	kinase, ankyrin	3	16	0	0	38
GL50803_15218	WD-40 repeat protein		WD40	9	0	0	0	0
GL50803_101326	hypothetical protein		none	0	8	0	0	0
GL50803_15918	hypothetical protein	25	none	3	0	0	0	0
GL50803_4977	Nek kinase GK282		kinase	3	0	0	0	0
GL50803_86815	hypothetical protein		none	0	0	0	0	0
GL50803_17053	ankyrin repeat protein	14	ankyrin	12	6	0	0	31
GL50803_13766	ankyrin repeat protein	93	ankyrin	7	9	0	0	14
GL50803_103807	ankyrin repeat protein	103	ankyrin	0	0	0	0	50
GL50803_13590	ankyrin repeat protein		ankyrin	0	0	0	0	0
GL50803_40016	ankyrin repeat protein		ankyrin	0	0	0	0	0
GL50803_4912	Nek kinase GK265		kinase	0	0	0	0	0
GL50803_3934	hypothetical protein		none	0	0	0	0	0
GL50803_15101	alpha17-giardin		annexin	0	0	0	0	0
GL50803_7797	alpha5-giardin		annexin	0	0	0	0	0
GL50803_5010	Ser/Thr Phos PP2A		calcineurin-like phosphoesterase	0	0	0	0	0
GL50803_92498	Nek kinase GK270		kinase	0	0	0	0	0
GL50803_14681	ankyrin repeat protein		ankyrin	20	3	0	0	0
GL50803_7414	ankyrin repeat protein		ankyrin	0	0	0	0	0
GL50803_5358	aurora kinase		kinase	0	0	0	0	0
GL50803_24321	Nek kinase GK261		kinase	8	0	0	0	0
GL50803_10181	hypothetical protein		none	0	0	0	0	0
GL50803_2556	hypothetical protein		none	0	0	0	0	0
GL50803_3760	ankyrin repeat protein		ankyrin	0	0	0	0	0
GL50803_17090	SAM domain protein		SAM	38	11	0	0	0
GL50803_16843	ankyrin repeat protein		ankyrin	0	0	0	0	0
GL50803_14551	alpha6-giardin	33	annexin	66	0	0	0	0
GL50803_10038	alpha18-giardin	32	annexin	0	0	0	0	19
GL50803_5375	Nek kinase GK170	45	kinase	15	7	0	0	10

GL50803_16804	dynein heavy chain	262	DHC	10	1	0	0	7
GL50803_33218	dynein intermediate chain IC78	84	DIC	9	4	0	0	19
GL50803_17243	OAD-beta dynein	163	DHC	6	0	0	0	9
GL50803_17265	OAD-alpha dynein	302	DHC	5	0	0	0	15
GL50803_6939	dynein intermediate chain IC70	70	DIC	2	1	0	0	11
GL50803_113677	hypothetical protein	255	none	97	35	0	0	18
GL50803_115478	hypothetical protein	80	none	55	5	0	0	0
GL50803_11390	Nek kinase GK209	85	kinase	36	7	0	0	0
GL50803_8217	uridine kinase	66	PRK	35	0	0	0	0
GL50803_11118	enolase	48	enolase	34	2	0	0	6
GL50803_7031	hypothetical protein	109	none	26	13	0	0	0
GL50803_93551	metalloprotease	129	M16C protease	21	2	0	0	0
GL50803_15953	Nek kinase GK231	125	kinase	20	0	0	0	39
GL50803_9720	ankyrin repeat protein	113	ankyrin	19	3	0	0	28
GL50803_9508	metalloprotease	131	insulinase	19	3	0	0	16
GL50803_21444	hypothetical protein	66	none	18	14	0	0	34
GL50803_14895	hypothetical protein	72	none	17	4	0	0	21
GL50803_16926	hypothetical protein	57	none	15	7	0	0	0
GL50803_103059	dynein heavy chain	274	DHC	15	4	0	0	29
GL50803_16549	uridine kinase	77	PRK	15	2	0	0	0
GL50803_114462	axonemal p66 (RSP6)	63	ODA-DC 2	11	5	0	0	6
GL50803_112112	hypothetical protein	136	none	11	3	0	0	40
GL50803_7207	hypothetical protein	120	none	9	2	0	0	0
GL50803_32999	hypothetical protein	51	none	8	1	0	0	0
GL50803_102034	Nek kinase GK295	108	kinase	7	0	0	0	0
GL50803_11164	ankyrin repeat protein	79	ankyrin	6	16	0	0	22
GL50803_102023	ankyrin repeat protein	92	ankyrin	6	0	0	0	0
GL50803_33660	ankyrin repeat protein	104	ankyrin	5	7	0	0	0
GL50803_17568	ankyrin repeat protein	60	ankyrin	5	3	0	0	7
GL50803_6081	ankyrin repeat protein	132	ankyrin	5	0	0	0	25
GL50803_11720	ankyrin repeat protein	48	ankyrin	5	0	0	0	0
GL50803_15446	hypothetical protein	38	none	5	0	0	0	0
GL50803_95192	ankyrin repeat protein	124	ankyrin	4	2	0	0	0

GL50803_26199	Nek kinase GK262	53	kinase	4	1	0	0	0
GL50803_93294	ankyrin repeat protein	139	ankyrin	3	5	0	0	0
GL50803_15054	kelch repeat protein	166	kelch repeat	3	2	0	0	0
GL50803_14742	Nek kinase GK253	33	kinase	3	1	0	0	0
GL50803_8174	ankyrin repeat protein	94	ankyrin	2	5	0	0	71
GL50803_16998	conserved hypothetical protein	69	none	2	5	0	0	0
GL50803_16543	hypothetical protein	64	none	2	3	0	0	5
GL50803_13467	hypothetical protein	35	none	2	1	0	0	0
GL50803_11604	hypothetical protein	35	none	2	0	0	0	0
GL50803_12224	hypothetical protein	35	none	2	0	0	0	0
GL50803_4624	DUF4490 domain protein	15	DUF4490	1	7	0	0	0
GL50803_95787	hypothetical protein	147	none	1	4	0	0	18
GL50803_13133	hypothetical protein	60	none	0	14	0	0	40
GL50803_5333	calmodulin	17	EF-hand	0	14	0	0	35
GL50803_9861	hypothetical protein	43	none	0	2	0	0	15
GL50803_3746	hypothetical protein	119	none	0	1	0	0	12
GL50803_16332	hypothetical protein	196	none	0	0	0	0	17
GL50803_86761	hypothetical protein	79	none	0	0	0	0	17
GL50803_16833	EGF-like domain containing protein	65	EGF-like domain	0	0	0	0	16
GL50803_14341	hypothetical protein	28	none	0	0	0	0	8
GL50803_3762	ankyrin repeat protein	82	ankyrin	0	0	0	0	5
GL50803_14345	hypothetical protein	160	none	0	0	0	0	0
GL50803_13437	ankyrin repeat protein	35	ankyrin	0	0	0	0	0
GL50803_15587	ankyrin repeat protein	28	ankyrin	0	0	0	0	0
GL50803_16729	hypothetical protein	41	none	0	0	0	0	0
GL50803_17375	hypothetical protein	41	none	0	0	0	0	0
GL50803_29796	hypothetical protein	41	none	0	0	0	0	0
GL50803_14583	hypothetical protein	21	none	0	0	0	0	0
GL50803_14507	hypothetical protein	43	none	0	0	0	0	0
GL50803_4692	hypothetical protein	27	none	0	0	0	0	0
GL50803_15605	hypothetical protein	43	none	0	0	0	0	0
GL50803_112079	alpha-tubulin 2	51	tubulin					

CB3	P3	localization	EM	body	DM	LC	OZ	VG	DB	MB	FL	cyFL	bb	REF	other localization	DAP
153	239	antibody	MR	disc			OZ	VG						[77]		DAP
94	72	C-term GFP	MT/OZ	disc	DM		OZ	VG		MB				[7]		DAP
69	124	antibody		disc			OZ	VG						[30]		DAP
69	33	C-term GFP	MR	disc			OZ	VG						this study	none	DAP
46	21	C-term GFP			DM		OZ	VG						this study	none	DAP
560	19	C-term GFP												this study	cytoplasm	CY
42	25	C-term GFP	MR	disc			OZ	VG						this study	none	DAP
10	13	HA tag		disc	DM									[76]		DAP
26	10	none												this study		nd
147	0	C-term GFP		disc			OZ							this study	no VG	DAP
55	25	none												this study		nd
28	29	none												this study		nd
15	33	C-term GFP		disc			OZ							this study	no VG	DAP
98	19	C-term GFP		disc			OZ							this study	no VG	DAP
92	3	none												this study		nd
30	7	C-term GFP		disc	DM		OZ			MB		cyFL		this study	cytoplasmic caudal axoneme	DAP
66	24	C-term GFP		disc			OZ			MB				this study	no VG?	DAP
5	0	C-term GFP			DM			VG						this study	none	DAP
22	3	C-term GFP		disc			OZ	VG		MB				this study		DAP
6	0	none												this study		nd
38	25	none												this study		nd
22	6	none												this study		nd
9	25	C-term GFP												this study	no localization	NO
37	7	C-term GFP			DM							cyFL	BB	this study		DAP
43	19	C-term GFP		disc			OZ		DB	MB				this study		DAP
5	19	none												this study		nd
5	5	none												this study		nd
34	14	C-term GFP		disc			OZ	VG		MB				this study		DAP
13	2	C-term GFP			DM					MB		cyFL		[7]	cytoplasmic anterior axonemes	DAP
14	36	C-term GFP			DM				DB					this study		DAP
7	5	C-term GFP		disc			OZ	VG						this study	none	DAP
0	5	C-term GFP		disc				VG						this study	none	DAP

6	9	C-term GFP			DM				MB	FL			this study	all flagella	DAP
122	2	C-term GFP											this study	plasma membrane	PM
7	0	C-term GFP		disc		OZ	VG						this study	cytoplasm	DAP
7	5	none											this study		nd
19	11	C-term GFP			DM							BB	[7]	no ventral groove	DAP
68	0	C-term GFP									cyFL		this study	all cytoplasmic axonemes	FL
5	21	C-term GFP			DM				MB	FL			this study	all flagella	DAP
0	5	C-term GFP			DM				MB	FL			this study	all flagella	DAP
113	0	C-term GFP											this study	cytoplasm	CY
5	8	C-term GFP			DM				MB	FL			this study	all flagella	DAP
8	2	C-term GFP								FL			this study	all flagella	FL
8	16	none											this study		nd
5	8	C-term GFP							MB	FL			this study		FL
6	3	AU1 tag		disc								BB	[75]		DAP
11	20	C-term GFP											this study	no localization	NO
17	2	C-term GFP								FL			this study	all flagella	FL
5	8	none											this study		nd
67	0	AU1											[34]	plasma membrane	PM
18	0	C-term GFP											this study	no localization	NO
8	2	C-term GFP										BB	this study		BB
3	0	C-term GFP					VG						this study	none	DAP
11	0	C-term GFP				OZ		DB			cyFL		[7]	cytoplasmic caudal axonemes	DAP
9	0	C-term GFP			DM				MB		cyFL	BB	this study	caudal cytoplasmic axonemes	DAP
0	0	C-term GFP		disc	DM	OZ			MB		cyFL		this study	all cytoplasmic axonemes	DAP
235	179	antibody	MT	disc	DM	OZ	VG	DB	MB	FL	cyFL		[78]		MT
122	75	antibody	MT	disc	DM	OZ	VG	DB	MB	FL	cyFL		[78]		MT
151	0	C-term GFP								FL			this study	plasma membrane, all flagella	FL
182	0	none											this study		nd
44	0	C-term GFP											this study	plasma membrane	PM
195	0	none											this study	no localization	NO
32	0	C-term GFP		disc			VG			FL			[15]	ventral flagella	DAP
28	0	none											[34]	lethal?	nd
71	0	C-term GFP											this study	plasma membrane	PM

8	20	none										this study	no localization	NO
4	0	HA tag										25057014		nd
2	0	none										this study		nd
11	0	C-term GFP		DM							BB	[7]		DAP
49	0	C-term GFP										this study	cytoplasm	CY
12	24	none										this study		nd
21	0	C-term GFP										this study	plasma membrane	PM
6	0	C-term GFP							FL			this study	marginal plates; ciliary pockets	FL
6	0	none										this study		nd
6	2	C-term GFP								cyFL	BB	this study		FL
0	0	C-term GFP					DB					this study	none	DAP
0	0	C-term GFP					DB	MB				this study	cytoplasm	DAP
0	0	C-term GFP					DB	MB		cyFL		this study	all cytoplasmic axonemes	DAP
0	0	C-term GFP					DB					this study	none	DAP
0	0	C-term GFP	disc	DM	OZ	VG						[7]	none	DAP
0	0	AU1 tag	disc	DM		VG						[34]		DAP
0	0	HA tag	disc	DM								[74]		DAP
0	0	C-term GFP		DM	OZ	VG		MB				this study		DAP
0	0	C-term GFP		DM	OZ	VG		MB				this study		DAP
0	0	antibody		DM		VG						[55]		DAP
9	0	C-term GFP		DM		VG						[7]	none	DAP
0	0	C-term GFP		DM		VG						this study	none	DAP
0	0	C-term GFP		DM		VG						this study	none	DAP
0	0	C-term GFP		DM								[7]	none	DAP
6	0	C-term GFP		DM								[7]	none	DAP
0	0	C-term GFP		DM								[7]	bare area	DAP
0	0	C-term GFP		DM								[7]	bare area	DAP
7	0	C-term GFP		DM								this study	no VG	DAP
0	0	C-term GFP		DM								this study	marginal plates	DAP
0	0	C-term GFP		DM								this study	none. no VG	DAP
0	0	C-term GFP		DM						cyFL	BB	this study	caudal cytoplasmic axonemes	DAP
0	0	C-term GFP		DM						cyFL	BB	this study	all cytoplasmic axonemes, cytoplasm	DAP
0	0	C-term GFP		DM						cyFL	BB	this study	all cytoplasmic axonemes	DAP

0	0	C-term GFP		DM				MB		cyFL		this study	all cytoplasmic axonemes	DAP
0	0	C-term GFP		DM						cyFL		this study	cytoplasmic posteriolateral axonemes	DAP
0	0	C-term GFP		DM								this study	cytoplasm	DAP
0	0	C-term GFP			LC							[7]	none	DAP
10	0	C-term GFP			LC							[7]	none	DAP
0	0	C-term GFP			LC					cyFL		this study	all cytoplasmic axonemes, cytoplasm	DAP
0	0	C-term GFP			LC					cyFL	BB	this study	all cytoplasmic axonemes, cytoplasm	DAP
11	16	C-term GFP	disc			OZ	VG					this study	none	DAP
0	0	C-term GFP	disc			OZ	VG					this study	none	DAP
0	0	C-term GFP	disc			OZ	VG	MB				this study	median body, cytoplasm	DAP
12	0	C-term GFP	disc			OZ						[7]	none. no VG	DAP
5	0	C-term GFP	disc			OZ						[7]	no ventral groove	DAP
7	0	C-term GFP	disc			OZ						[7]	none	DAP
0	0	C-term GFP	disc			OZ				cyFL		this study	cytoplasmic anterior axonemes	DAP
0	0	C-term GFP	disc			OZ		MB				this study		DAP
0	0	C-term GFP	disc			OZ		MB				this study	no VG	DAP
0	0	C-term GFP	disc			OZ		MB				this study	no VG	DAP
0	0	AU1 tag	disc				VG		FL			[34]	ventral flagella	DAP
0	0	AU1 tag	disc				VG		FL			[34]	ventral flagella	DAP
0	0	antibody	disc				VG				BB	[73]		DAP
0	0	AU1 tag	disc				VG			cyFL	BB	[75]	anterior axonemes	DAP
0	0	C-term GFP	disc				VG			cyFL	BB	this study	all cytoplasmic axonemes, no nuclei	DAP
0	0	C-term GFP	disc				VG					this study	none	DAP
0	0	antibody	disc									[53]		DAP
0	0	C-term GFP	disc									[7]	none. no VG	DAP
0	0	C-term GFP	disc							cyFL		this study	all cytoplasmic axonemes	DAP
0	0	C-term GFP	disc					MB	FL	cyFL		this study	all flagella	DAP
0	0	C-term GFP	disc									this study	cytoplasm	DAP
0	0	C-term GFP				OZ				cyFL	BB	[7]	snMTs?	DAP
0	0	C-term GFP				OZ						this study	none	DAP
11	0											[34]	cytoplasm	CY
6	0	none										[34]		nd
6	0	none										REF		nd

10	0	none					REF		nd
9	0	none					REF		nd
7	0	none					REF		nd
15	0	none					REF		nd
5	0	none					REF		nd
166	0	none					this study		nd
88	0	none					this study		nd
18	0	C-term GFP					this study	plasma membrane	PM
10	0	none					this study		nd
24	0	none					this study		nd
18	0	none					this study		nd
16	0	none					this study		nd
22	0	none					this study		nd
23	0	none					this study		nd
31	0	none					this study		nd
54	0	none					this study		nd
28	0	none					this study		nd
2	3	none					this study		nd
17	0	none					this study		nd
9	0	none					this study		nd
2	5	C-term GFP		FL			this study	all flagella	FL
28	0	none					this study		nd
0	5	none					this study		nd
17	0	none					this study		nd
13	0	none					this study		nd
11	0	none					this study		nd
5	0	C-term GFP			cyFL		this study		FL
21	0	C-term GFP					this study	plasma membrane	PM
6	0	none					this study		nd
13	0	none					this study		MT
6	0	C-term GFP					this study	plasma membrane	PM
3	7	C-term GFP	MB		cyFL	BB	this study		FL
5	0	none					this study		nd

9	0	none											this study		nd
17	0	none											this study		nd
6	0	C-term GFP									cyFL		this study	cytoplasmic caudal and posteriolateral axonemes	FL
13	0	C-term GFP											this study	plasma membrane	PM
24	0	C-term GFP											this study	no localization	NO
0	3	C-term GFP								FL			this study	all flagella	FL
10	0	none											this study		nd
2	7	none											this study		nd
2	8	none											this study		nd
0	7	C-term GFP							MB				this study		MB
0	5	C-term GFP							MB		cyFL	BB	this study	all cytoplasmic axonemes	FL
5	0	none											this study		nd
10	0	C-term GFP							MB	FL			this study		FL
8	0	C-term GFP										BB	this study	plasma membrane	BB
9	0	none											this study		nd
11	0	none											this study		nd
18	0	none											this study		nd
16	0	none											this study		nd
10	0	none											this study		nd
5	0	none											this study		nd
15	0	none											this study		nd
12	0	none											this study		nd
6	0	none											this study		nd
6	0	none											this study		nd
5	0	none											this study		nd
2	7	none											this study		nd
0	6	C-term GFP							MB	FL		BB	this study	anterior flagella, caudal flagella	FL
0	6	C-term GFP							MB		cyFL		this study	all cytoplasmic axonemes	FL
0	10	none											this study		nd
0	7	none											this study		nd
0	5	none											this study		nd
		antibody	MT	disc	DM	OZ	VG	DB	MB	FL	cyFL		[78]		MT